


## ORIGINAL RESEARCH

# Stronger conservation promotes mangrove biomass accumulation: Insights from spatially explicit assessments using UAV and Landsat data

Zhu Zhu<sup>1,2</sup>, Minmin Huang<sup>1,2</sup>, Zeyou Zhou<sup>3</sup>, Guixiang Chen<sup>4</sup> & Xudong Zhu<sup>1,2,5</sup> 

<sup>1</sup>State Key Laboratory of Marine Environment Science, Key Laboratory of the Coastal and Wetland Ecosystems (Ministry of Education), Coastal and Ocean Management Institute, College of the Environment and Ecology, Xiamen University, Xiamen, Fujian 361102, China

<sup>2</sup>National Observation and Research Station for the Taiwan Strait Marine Ecosystem (Xiamen University), Zhangzhou, Fujian 361102, China

<sup>3</sup>Fujian Environmental Protection Design Institute Company Limited, Fuzhou, Fujian 350025, China

<sup>4</sup>Administrative Bureau of Zhangjiang Estuary Mangrove National Nature Reserve, Zhangzhou, Fujian 363300, China

<sup>5</sup>Southern Marine Science and Engineering Guangdong Laboratory (Zhuhai), Zhuhai, Guangdong 519000, China

## Keywords

aboveground biomass, canopy height, enhanced vegetation index, stand age, structure from motion, unmanned aerial vehicle

## Correspondence

Xudong Zhu, College of the Environment and Ecology, Xiamen University, Xiamen, Fujian 361102, China. Tel: +86-592-2880206; Fax: +86-10-2880206; E-mail: xdzhu@xmu.edu.cn

Editor: Mat Disney

Received: 19 October 2021; Revised: 17 March 2022; Accepted: 29 March 2022

doi: 10.1002/rse2.268

## Abstract

Chinese mangroves have been recovered in area over the past two decades from previous declining trend, and about half of existing mangroves are still in their young growth stage. This provides a unique opportunity to assess mangrove conservation by examining the growth dynamics of young mangroves over different conservation periods. However, we are currently short of effective assessment tools for spatially explicit quantification of mangrove conservation effects. To fill up this gap, we proposed a novel remote sensing approach using readily available unmanned aerial vehicle (UAV) and Landsat enhanced vegetation index (EVI) data to assess the spatial evolution of aboveground biomass (AGB) of young mangroves. With the space-for-time hypothesis, the approach implemented with an empirical EVI-height-AGB equation was tested in four subtropical estuarine mangroves in the southeastern coast of China. The results indicated: (a) the UAV-based Structure from Motion (SfM) technology served as an effective and low-cost means for capturing the spatial heterogeneity of mangrove canopy heights; (b) a maximum stand age of 15 years could be used to define the young growth stage of mangroves, for which the EVI-height relationships could be described by exponential equations without suffering significant spectral saturation effects; (c) mangrove forests had overall faster annual AGB accumulation during the young growth stage over the post-2000 *versus* pre-2000 conservation period. This study is one of the first attempts to develop a remote sensing approach for quantifying spatially explicit AGB accumulation rates of young mangroves. It highlights the practicability and advantage of the UAV-SfM technology and confirms that stronger conservation efforts promote mangrove AGB accumulation over the past two decades. The developed EVI-height-AGB framework fueled with readily available UAV and Landsat data provides a unique tool for assessing mangrove conservation effects from landscape to regional scales.

## Introduction

Mangrove forests, one of the most productive ecosystems, are distributed in the tropical and subtropical coasts (Alongi, 2009; Giri et al., 2011). Mangrove forests have far-ranging environmental services and critical ecological

functions including provisional, regulating, cultural, supporting aspects (Barbier, 2016; Ferreira et al., 2015; James et al., 2013; Uddin et al., 2015). For example, as one of the most carbon-rich ecosystems (Donato et al., 2011), mangroves export 10% of the terrestrial dissolved organic carbon to the ocean (Dittmar et al., 2006) with covering

only 0.1% of the earth's continental surface. Organic carbon in mangrove areas is mainly stored in biomass and sediments (Kauffman et al., 2014), and management actions including conservation and restoration can reduce the loss of carbon stocks in mangroves (Vanderklift et al., 2019). To better implement these management actions, fundamental knowledge and scientific guidance are crucially significant (Farzanmanesh et al., 2021). As one of the most important indicators of mangrove biotic and abiotic processes such as productivity, carbon burials, sediment trapping, bio-geomorphological feedbacks, aboveground biomass (AGB) has received much more attentions (Kirwan & Megonigal, 2013; Klemas, 2013; Pham et al., 2019). Therefore, many studies have quantified mangrove AGB, based on field inventory or remote sensing approaches, to assess the role of mangroves in the global carbon cycle (Castillo et al., 2017; Doughty et al., 2021; Hu et al., 2020; Lu, 2005; Navarro et al., 2020; Salum et al., 2020; Wang et al., 2020a).

More than half of Chinese mangroves have been lost by the early 1990s, after which Chinese government has made much greater efforts on mangrove conservation and restoration (Chen et al., 2009; Hu et al., 2018; Jia et al., 2018; Jia et al., 2021). As a consequence, the areal extent of Chinese mangroves stopped declining and began to increase from *ca.* 2000 (Jia et al., 2018; Jia et al., 2021; Wang et al., 2020b). It was reported that young mangroves accounted for *ca.* 50% of the existing mangrove area in China (Hu et al., 2018; Jia et al., 2018). Most of the previous remote sensing-based mangrove studies examine mangrove extent and species across temporal and spatial scales (Hu et al., 2018; Jia et al., 2018; Wang et al., 2019; Zhao & Qin, 2020), but less focus on mapping and assessing the spatio-temporal dynamics of young mangroves in particular for AGB (Wang et al., 2018; Wang et al., 2021). This can be partially explained by the lack of effective and low-cost remote sensing assessment tools, representing a critical knowledge gap in terms of evaluating the effects of mangrove conservation and restoration.

In comparison with field inventory on mangroves, remote sensing techniques with satellite and aerial platforms are more cost-effective and efficient in collecting mangrove data, especially at large spatial or long temporal scales (Jones et al., 2020; Navarro et al., 2020). Readily available satellite data such as Landsat imagery have been widely used for spatially explicit assessments of mangrove AGB (Hickey et al., 2018; Pflugmacher et al., 2014), but these applications could suffer from large uncertainty since satellite data often fail to acquire canopy structure information that is key for mangrove AGB retrievals. To improve the estimation of mangrove AGB, recent studies have integrated point cloud data from aerial LiDAR system (ALS) with field inventory and satellite imagery, but high costs of ALS campaigns

prohibit extensive applications (Doughty et al., 2021; Zhu et al., 2019). Over the past decade, the Structure-from-Motion (SfM) method with unmanned aerial vehicle (UAV) flights has been widely used for retrieving canopy structure information like canopy height models (CHM) in various ecosystems including mangrove forests (Lucas et al., 2020; Navarro et al., 2020; Otero et al., 2018). For example, Otero et al. (2018) suggested the SfM method was very useful for retrieving CHM and AGB of mangrove forests with a single dominant layer. The SfM method has the potential to improve the efficiency of collecting spatial data (Dandois & Ellis, 2013; Messinger et al., 2016), acquire a finer spatial resolution than satellite data (Navarro et al., 2020) and provide a low-cost alternative option of ALS with comparable accuracy (Sankey et al., 2017).

The synergetic changes in canopy structure parameters and remote sensing vegetation indices with stand age lay a foundation for deriving mangrove canopy structures from vegetation indices (Lee, 2008; Thi Kim Cuc & Thi Hien, 2021). Normalized difference vegetation index (NDVI) and enhanced vegetation index (EVI) are often used in remote sensing studies on biomass estimations (Doughty et al., 2021; Wang et al., 2020a), while EVI could be more sensitive to AGB variation in particular for high-biomass ecosystems since it is less affected by the spectral saturation effect (Huete et al., 2002). It is reported that canopy height is closely correlated with both EVI and AGB (Saenger & Snedaker, 1993; Waring et al., 2006), and thus canopy height could serve as a bridge for retrieving AGB from EVI. Therefore, the combination of readily available Landsat EVI and SfM-based canopy heights could provide a novel remote sensing approach for assessing long-term evolution of mangrove AGB on the decadal time scale.

As far as we know, there is no such study focusing on decade-scale AGB dynamics of young mangroves in a spatially explicit manner. A remote sensing reconstruction of the historical evolution of mangrove AGB could help close this knowledge gap. In this study, we aim to examine the benefits of mangrove conservation in terms of AGB accumulation rates for both pre-2000 and post-2000 periods. The specific objectives of this study are (1) to demonstrate the practicability of the SfM method in estimating mangrove canopy heights; (2) to develop an empirical EVI-height-AGB relationship to map annual mangrove AGB; and (3) to assess spatial and temporal evolutions of mangrove AGB accumulation rates.

## Materials and Methods

### Overview

To conduct spatially explicit assessments of mangrove AGB accumulation, we developed a remote sensing

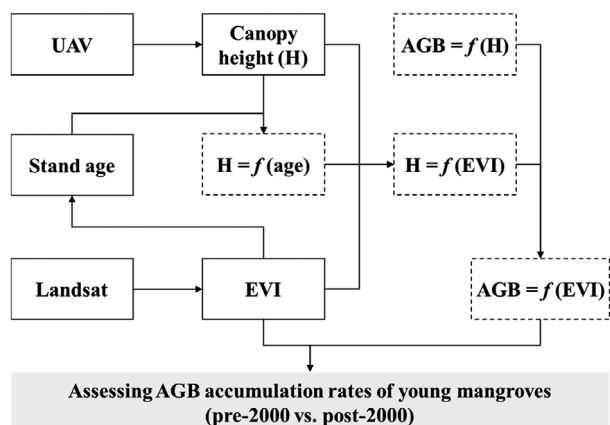


**Figure 1.** Overview of the remote sensing-based approach for modeling and assessing AGB accumulation rates of young mangroves. Solid boxes denote data sources and derived products, while dashed boxes denote empirical functions used for retrieving AGB.

estimation approach for AGB of young mangroves using readily available Landsat and UAV imagery (Fig. 1). By assuming an exponential EVI-height relationship and a linear height-AGB relationship, we generated an empirical EVI-height-AGB equation to assess AGB accumulation of young mangroves using Landsat EVI data only. To reduce the impact of spectral saturation effect on the EVI-height relationship, we limited the analyses to the young growth stage of mangroves. The age threshold used for differentiating young from the mature stage was determined by the age-height growth curve based on a space-for-time or chronosequence analysis, where stand age was derived from time series Landsat imagery and canopy height was estimated by SfM-based CHM. The widely used space-for-time analysis in ecological studies assumes that spatial phenomena can be used to model temporal processes that are unobservable (Blois et al., 2013), and the analysis has often been applied in mangrove studies to examine the relationships between biomass and stand age (Thi Kim Cuc & Thi Hien, 2021; Walcker et al., 2018) and between growth and environmental factors (Azman et al., 2021).

### Mangrove study sites

The remote sensing approach for estimating AGB was tested in four estuarine mangrove sites in the southern coast of Fujian province, China, located in (from south to north) Zhangjiang Estuary (ZJE), Jiulong River Estuary (JRE), Xiamen Bay (XMB) and Quanzhou Bay (QZB) (Fig. 2). The mangrove area of these four sites accounts for >90% of the total mangrove area of Fujian province. These mangrove forests are located near the northern border of their natural distribution in China and mainly

comprised of *Kandelia obovata*, *Avicennia marina* and *Aegiceras corniculatum*. Three of these sites are located within national (ZJE) or provincial (JRE and QZB) nature reserves and another one (XMB) is located within a restored mangrove wetland park. With longer conservation history, mangrove forests in ZJE and JRE are generally older and more structurally complex than those in XMB and QZB. The stand age of mangrove forests is related with the conservation history: JRE and QZB are provincial nature reserves established in 1988 and 2003, respectively, while ZJE was first established as a provincial nature reserve in 1990 and then promoted to a national one in 2003. As a result, many of mangrove forests are older than 35 years old in ZJE and JRE (Fig. 2C-D) and younger than 19 years old in QZB (Fig. 2F), while XMB, a restored wetland since 2010, has the youngest mangrove forests (<7 years old) among these four sites (Fig. 2E). These mangrove sites experience semi-diurnal tides and a subtropical monsoon climate with a wet season over April ~ September and a dry season over October ~ March.

### Mangrove stand age and canopy height

Time series of 30-m Landsat surface reflectance data were used to generate annual EVI and resultant stand age of mangrove forests by 2020. All available Landsat surface reflectance ( $\rho$ ) data from USGS Landsat Level-1 Tier 1 data products were used to calculate EVI (Huete et al., 2002):

$$EVI = 2.5 \times \frac{\rho_{nir} - \rho_{red}}{\rho_{nir} + 6 \times \rho_{red} - 7.5 \times \rho_{blue} + 1} \quad (1)$$

The Tier 1 data products are considered suitable for time series pixel-level analysis since the data have well-characterized radiometry and are inter-calibrated across different Landsat instruments. To ensure high-quality surface reflectance data, a series of quality control procedures were applied including atmospheric correction and pixel removals contaminated by cloud or shadow (Foga et al., 2017; Masek et al., 2006; Vermote et al., 2016). Following previous studies (Berveglieri et al., 2021; Potapov et al., 2012; Younes et al., 2020), we used the median of all quality-controlled EVI values within a year to represent annual EVI, aiming to reduce the disturbances from atmospheric, tidal and seasonal variations. A summary of the acquisition dates and number of all available EVI images for each wetland can be found in Figure S3. The EVI calculation and quality control procedures were implemented using Google Earth Engine.

Annual EVI data were used to map the distribution of mangrove stand age. Following Chen et al. (2017) and their mangrove map as spatial constraints, a threshold

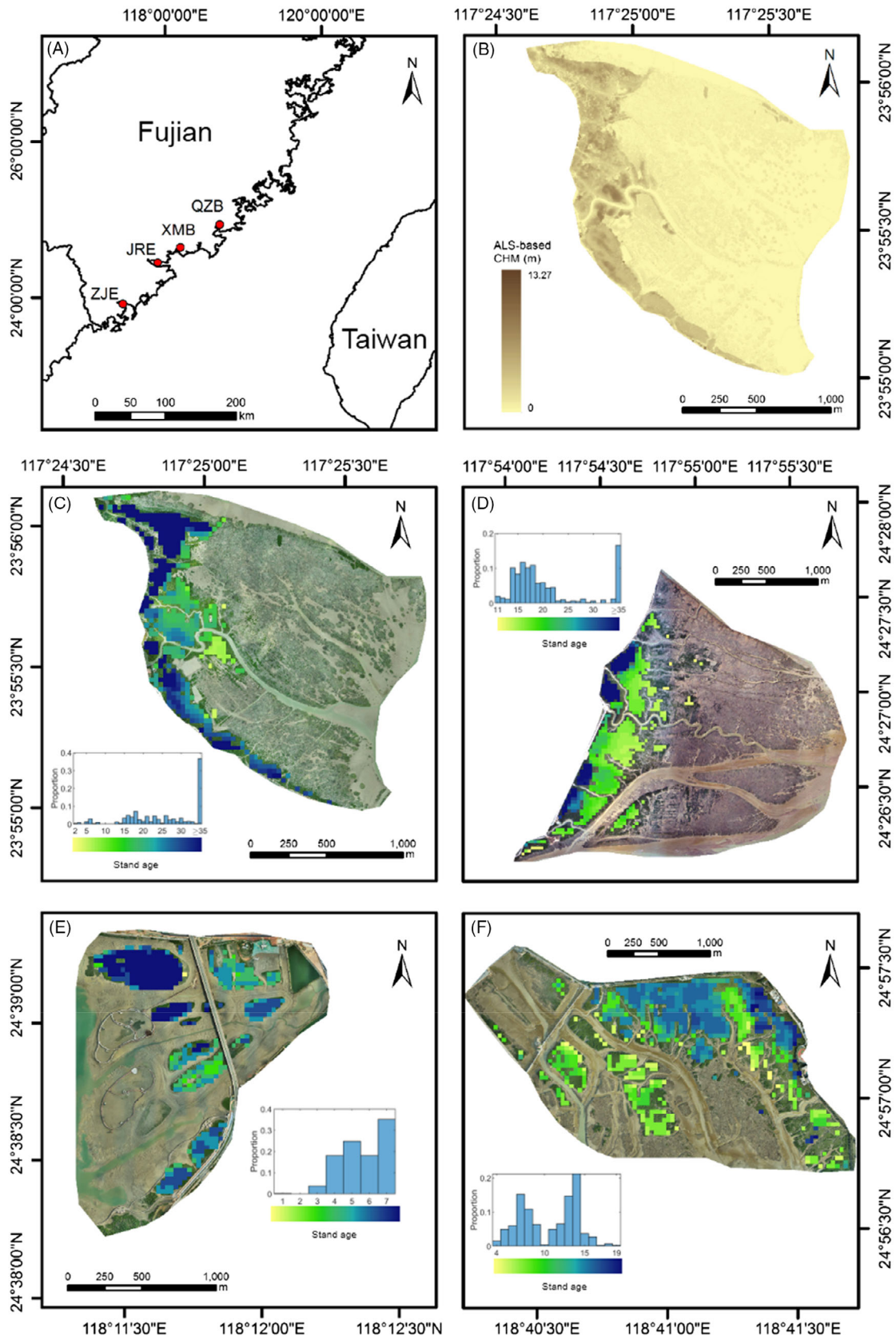


**Figure 2.** Locations of four mangrove sites (A) and their Landsat-based mapping of stand age by 2020 (C: Zhangjiang Estuary (ZJE), D: Jiulong River Estuary (JRE), E: Xiamen Bay (XMB), F: Quanzhou Bay (QZB)). UAV imagery acquired in 2020 or 2021 is used as the base map for each mangrove site, inset with the histogram of stand age. The canopy height model derived from airborne LIDAR system (ALS-based CHM) is also shown for ZJE (B).

criterion of  $EVI > 0.2$  was used to map mangrove pixels annually from 1986 to 2020. For each mangrove pixel in 2020, its stand age was calculated as the number of years since the earliest year labeled as mangrove for this pixel. The resultant stand age of mangrove pixels ranged from 1 year (*i.e.* 2020 as the first year labeled as mangrove) to 35 years (labeled as mangrove for all the years). Note that mangrove pixels of 35 years or older were not differentiated in this study due to the lack of sufficient data in prior to 1986.

Mangrove canopy heights used in this study were derived from two data sources including the ALS-based CHM for ZJE and the SfM-based CHMs for all sites. The ALS-based CHM, well-recognized high-accuracy canopy height data (Hickey et al., 2018; Lu et al., 2012; Salum et al., 2020), was treated as “true” values used for assessing the accuracy of SfM-based CHMs for ZJE, while the SfM-based CHM was used to formulate the age-height and EVI-height relationships for all sites. The ALS-based CHM was calculated as the difference between digital surface model (DSM) and digital terrain model (DTM) derived from LiDAR point cloud of ZJE acquired in 2017 at a point density of *ca.* 100 points/m<sup>2</sup> (Zhu et al., 2019). For each site, UAV (model: Phantom 4-RTK; DJI Technology, Shenzhen, China) flights at a height of *ca.* 200 m during low-tide periods were conducted to acquire a set of RGB images with high positioning accuracy over mangrove forests. Then, RGB images were mosaiced in Photoscan software (Agisoft LLC, St. Petersburg, Russia) to generate a high-resolution orthophoto (Fig. 2C-F) and a DSM based on the SfM algorithm, which is a widely used and effective 3-D reconstruction workflow that automatically identifies and ties common points on overlapping 2-D images to produce a 3-D point cloud (Schonberger & Frahm, 2016; Warfield & Leon, 2019). The CHM was derived from the DSM by subtracting a fixed base height through visually inspecting open bare mudflat (Lucas et al., 2020; Otero et al., 2018). All these CHMs from different data sources were spatially aligned and averaged to generate mean canopy height at the same spatial resolution as Landsat data. More information on ALS, UAV and Landsat data used in this study can be found in supplementary materials.

### Estimating above ground biomass (AGB)

Annual mangrove AGB maps were derived from Landsat EVI based on an empirical EVI-height-AGB equation, developed by fusing height-AGB and EVI-height

relationships. Following previous remote sensing studies on mangrove AGB (Fatoyinbo & Simard, 2013; Hickey et al., 2018), the linear height-AGB relationship from Saenger and Snedaker (1993) was applied to estimate mangrove AGB (Mg DW ha<sup>-1</sup>) from canopy height (H; m):

$$AGB = 10.8 \times H + 34.9 \quad (2)$$

The EVI-height relationship was developed by fitting an exponential equation using the SfM-based CHM and EVI:

$$H = a \times e^{b \times EVI} \quad (3)$$

where  $a$  and  $b$  are curve fitting parameters. To limit the EVI-height relationship into the young growth stage of mangroves, a threshold of maximum stand age was determined from the age-height growth curve using the space-for-time method. The logistic function was used to describe the increasing canopy height with stand age (year):

$$H = H_m / (1 + k_0 \times e^{-r \times AGE}) \quad (4)$$

where  $H_m$ ,  $k_0$  and  $r$  are curve fitting parameters, estimated by fitting the equation with the SfM-based CHM and EVI-derived stand age. The first (*i.e.* the beginning of the linear growth stage;  $AGE_{t1}$ ) and second (*i.e.* the ending of the linear growth stage;  $AGE_{t2}$ ) inflexion points of the growth curve were calculated following Gregorczyk (1991), and  $AGE_{t2}$  was used as the threshold of maximum stand age:

$$AGE_{t1} = (\ln(k_0) - 1.318) / r \quad (5)$$

$$AGE_{t2} = (\ln(k_0) + 1.318) / r \quad (6)$$

### Assessing AGB accumulation rates

Annual maps of mangrove AGB estimations for four mangrove sites were used to compare AGB accumulation rates between two conservation periods. With more extensive mangrove protections and establishments of natural reserves, the areal extent of mangroves in China overall changed from a declining period to an increasing period in *ca.* 2000 (Hu et al., 2018; Jia et al., 2018; Jia et al., 2021). Therefore, in this study, we divided the study period of 1986–2020 into pre-2000 and post-2000 conservation periods, and conducted spatially explicit comparisons of mangrove AGB accumulation rates during the young growth stage between these two periods. Specifically, for each

mangrove pixel of stand age  $\leq 20$  years by 2020 (post-2000 period), linear regression was applied to annual AGB time series over the linear growth stage ( $AGE_{t1} \leq AGE \leq AGE_{t2}$ ) to calculate a mean annual mangrove AGB accumulation rate; for each mangrove pixel of stand age  $>20$  years by 2020 (pre-2000 period), linear regression was applied to annual AGB time series over the linear growth stage before 2000.

## Results

### Mangrove stand age and canopy height maps

Mangrove stand age by 2020 was mapped for four mangrove sites (Fig. 2C-F). The exact stand age of mangroves  $\geq 35$  years old in ZJE and JRE cannot be identified and was thus simply labeled as  $\geq 35$  years. Mangroves of stand age  $\geq 35$  years accounted for 37% and 17% in ZJE and JRE, respectively. Among four mangrove sites, mangroves in ZJE had a more uniform distribution of stand

age from 2 to 35 years. For JRE, mangroves of stand age between 14 and 22 years had larger proportions than other ages. As recently restored wetlands, mangroves in both XMB and QZB were much younger. Mangroves in XMB were younger than 8 years old, while the distribution of mangrove stand ages in QZB, varying from 4 to 19 years old, had two peaks centered at 7 and 14 years old. The SfM-based CHM of mangrove pixels ( $y$ ) were closely correlated with the ALS-based CHM ( $x$ ; “true” canopy heights) in ZJE ( $y = 1.04x - 0.12$ ,  $R^2 = 0.67$ ,  $P < 0.01$ ; Fig. 3A). A cross-section through the ALS-based and SfM-based point clouds along a given mangrove transect (Fig. 3B) also confirmed that the two sets of CHM overall matched each other, with slight overestimation at the northern part of the transect (Fig. 3C).

### Mangrove stand age-height and EVI-height relationships

The space-for-time analyses indicated that spatially-mean mangrove canopy heights increased with stand

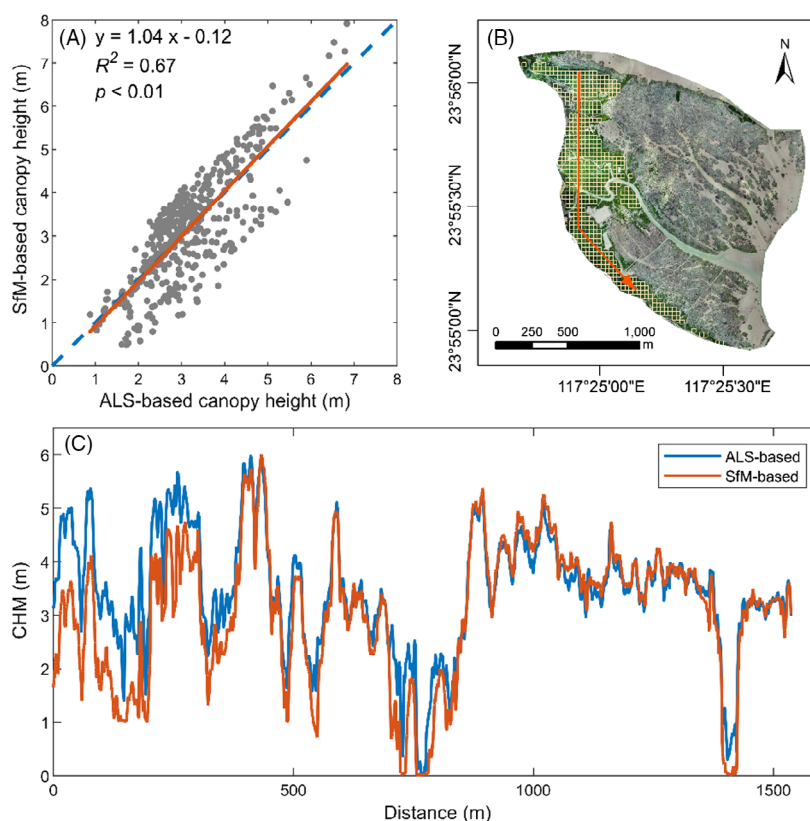


**Figure 3.** Comparison of mean canopy heights of 30-m mangrove pixels over the Zhangjiang Estuary between ALS-based CHM (Oct., 2017) and SfM-based CHM (Jan., 2019), with linear regression and one-to-one reference lines indicated by solid and dashed lines, respectively (A). The UAV imagery of the Zhangjiang Estuary overlaid by the grid cells of all these 30-m mangrove pixels is shown (B). A cross-section through the ALS-based and SfM-based point clouds is also shown for comparing the difference in CHM along the given transect running through main part of mangrove forests (the red arrow in (B)) (C).

age in four sites, but they differed in temporal evolution of the growth dynamics (Fig. 4). Although both ZJE and JRE had a similar variation range in stand age (data points of stand age  $\geq 35$  years were excluded in Fig. 4), JRE had the highest maximum canopy height up to 10 m (ca. 4 m higher than ZJE). Despite younger stand age  $< 20$  years, mangrove canopy heights in QZB (4 ~ 7 m) were similar to ZJE. As a recently restored mangrove wetland, XMB had both the youngest stand ages and the lowest canopy heights (2 ~ 5 m). Spatial variations of mangrove canopy heights (overall  $< 2$  m in terms of standard error) also changed with stand age in four sites. The logistic growth curves were fitted using spatially-mean canopy height and stand age. To ensure the performance, we only applied the logistic curves to formulate mangrove canopy height as a function of stand age for ZJE and JRE, which had enough variation ranges of stand age (Fig. 4A-B). The two inflexion points indicating the beginning and ending of

the linear growth stage were estimated as 5 and 13 years for ZJE (Fig. 4A) and 3 and 17 years for JRE (Fig. 4B). In this study, we used the averages of each inflexion point (4 and 15 years) at these two sites to define the linear growth stage, and mangroves of stand age  $< 4$  years and  $> 15$  years were excluded in further analyses on AGB accumulation rates. For young mangroves with stand age  $< 15$  years in four mangrove sites, mangrove canopy heights were positively correlated with Landsat EVI and their empirical relationships could be described by exponential equations (Fig. 5A-D). The performances of exponential equations differed among four sites with higher  $R^2$  in younger sites of QZB (0.57) and XMB (0.36) than older sites of ZJE (0.22) and JRE (0.13). Taking four sites together, a uniform empirical relationship between mangrove canopy height (H) and EVI was formulated (Fig. 5E;  $H = 1.75 \times e^{1.91 \times EVI}$ ,  $R^2 = 0.27$ ,  $P < 0.01$ ) and used for further mappings of annual mangrove AGB.

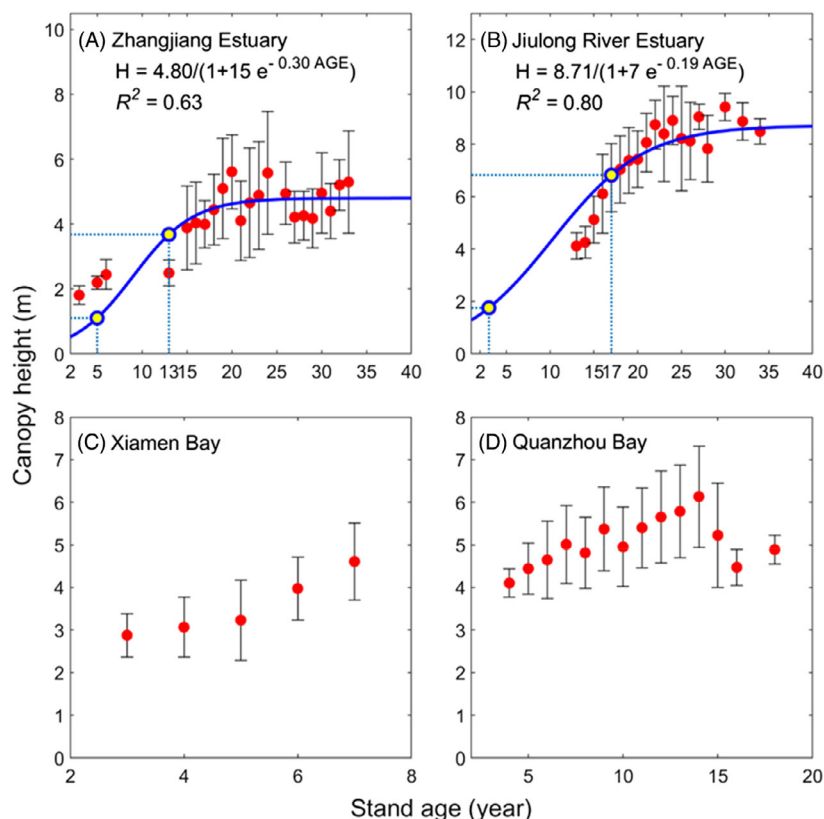


**Figure 4.** Spatially mean mangrove canopy height as a function of stand age in four mangrove sites (A–D). For each site, mangrove pixels were grouped by every stand age with solid dot and error bar, respectively, representing mean canopy height and standard error of pixels in each group. The logistic growth curves were used to fit empirical relationships between mean canopy height and stand age for ZJE and JRE with enough variation ranges of stand age. The beginning ( $AGE_{t1}$ ) and ending ( $AGE_{t2}$ ) points of the linear growth stage were also marked with circles for each fitted growth curve.

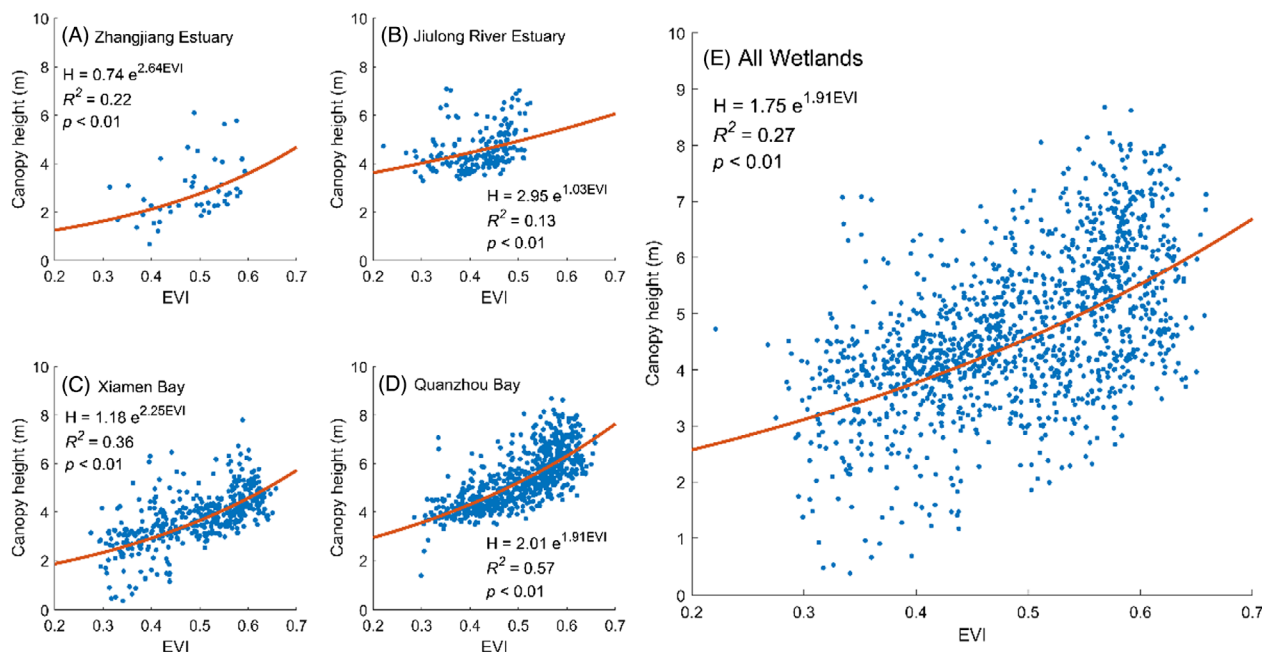


**Figure 5.** Relationships between SfM-based CHMs and Landsat EVI for young mangrove pixels (stand age < 15 years) in four sites (A–D) and all sites (E), fitted by the exponential EVI–height curves.

### Mangrove AGB accumulation rates

Annual maps of mangrove AGB were derived from Landsat EVI based on the uniform EVI–height–AGB empirical equation parameterized for these mangrove sites ( $AGB = 18.9 \times e^{1.91 \times EVI} + 34.9$ ). Although four mangrove sites had different forest growth histories and spatial distributions of stand age (Fig. 2), they shared a similar magnitude of spatially mean AGB in 2020 varying from  $80.70 \pm 3.50$  Mg DW ha<sup>-1</sup> in JRE to  $85.30 \pm 7.42$  Mg DW ha<sup>-1</sup> in QZB. For mangrove pixels established after 2000 only, four mangrove sites had overall similar increasing trends in spatially-mean mangrove AGB by 2020 (an increase of *ca.* 20 Mg DW ha<sup>-1</sup>; green lines in Fig. 6). For mangrove pixels established before 2000 only, inter-annual variation in spatially mean mangrove AGB over 1986–2020 differed between ZJE and JRE, with the former showing a more stable increasing trend (red lines in Fig. 6). Although these two groups of mangrove pixels had different initial levels of AGB (lower for the post-2000 group), both of them increased up to a similar level by 2020. Annual mangrove AGB accumulation rates in four sites during the young growth stage were mapped for the pre-2000 and post-2000 conservation periods (Fig. 7). For ZJE and JRE covering both periods, mangrove pixels established after 2000 only were mainly distributed in the seaward region. Although annual AGB accumulation rates in both periods had spatial

heterogeneity, the spatially mean value of annual rates over the post-2000 period (1.83 and 0.96 Mg DW ha<sup>-1</sup> y<sup>-1</sup> for ZJE and JRE, respectively) were overall higher than those over the pre-2000 period (1.18 and 0.33 Mg DW ha<sup>-1</sup> y<sup>-1</sup>). In comparison, younger XMB and QZB sites had obviously higher spatially mean annual AGB accumulation rates of 3.97 and 2.48 Mg DW ha<sup>-1</sup> y<sup>-1</sup>, respectively.

### Discussion

The application of SfM-based CHM for estimating mangrove canopy heights is unique, more effective, time saving and low cost (Dandois & Ellis, 2010; Navarro et al., 2020; Zarco-Tejada et al., 2014). First, in comparison with traditional field inventory, this method has the advantage to produce canopy height maps that are required for spatially explicit analyses. This uniqueness is highly necessary for capturing the spatial heterogeneity of canopy heights even within a single mangrove wetland (Zhu et al., 2019). Second, the comparison of performance in approximating ALS-based canopy heights by SfM-based CHMs confirms that the SfM method can well capture the spatial variation of mangrove canopy height. Third, only a few hours are needed by a single person to conduct field UAV flights and post-image processing (*e.g.* <4 hours required for covering a 50-ha mangrove wetland in ZJE), while it may cost much longer time and



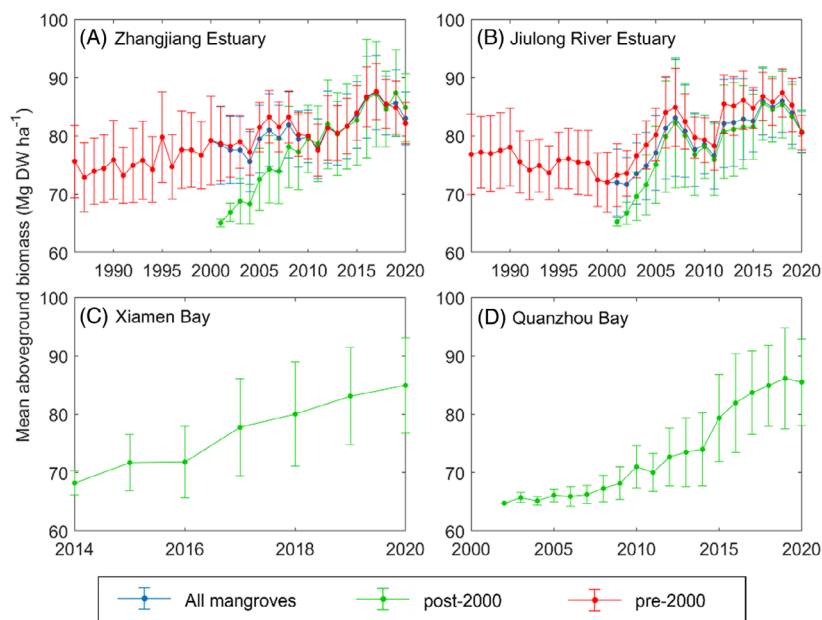


**Figure 6.** Temporal changes in spatially mean annual mangrove AGB (dots) and standard error (error bars) in four mangrove sites (A–D). The green lines for all sites denote annual time series of mangrove pixels established after 2000 only. The red lines (for ZJE and JRE only) denote annual time series of mangrove pixels established before 2000 only. The blue lines (for ZJE and JRE only) denote annual time series of all mangrove pixels over 2000–2020.

more persons to finish field inventory. Fourth, although the SfM-based CHM may bias from actual canopy heights due to the inability of the method to accurately characterize understory topography in particular for closed canopy, it costs much less than the ALS-based method and is thus more suitable for extensive applications (Lechner et al., 2020; Lucas et al., 2020; Otero et al., 2018).

The analyses of stand age–height relationships with the space-for-time method suggest that the threshold of maximum stand age can be used to differentiate young from mature stage of mangroves. With longer history of mangrove forests in ZJE and JRE (as natural reserves established in 1992 and 1988, respectively), mangroves in these two sites are more diverse in canopy structure and stand age. The estimated inflexion points of the logistic growth curves of these two sites indicate that canopy height increases with stand age before the first 15 years and then enters into mature stage with stable height. This stand age threshold is overall comparable with previous studies on mangrove growth dynamics with regards to stand age. Aksornkoae (1982) found mangroves took 15 years to reach the equilibrium of biomass in Thailand. Thi Kim Cuc and Thi Hien (2021) found that *K. obovata* might be still in the development stage at a 20-year stand age in northern Viet Nam. Mangroves in south Florida were found to reach their mature growth stage in 20–35 years (Davis, 1940). The difference among these stand age

thresholds is likely caused by site-dependent habitat and environmental conditions that determine the carrying capacity of mangroves (Shinozaki, 1961; Thi Kim Cuc & Thi Hien, 2021).

The exponential equations are found to well describe the EVI–height relationships during the young growth stage of mangroves, but the performance of the fitting curves differs among four sites. The lower performances in ZJE and JRE are mainly due to more uneven composition of mangrove stand age in these two older sites. Although these EVI–height relationships tend to be site-dependent, for the purpose of generality a uniform equation is applied to map annual mangrove AGB for all sites. The estimated AGB in these four mangrove sites are comparable with other estimations of subtropical mangrove forests ranging from 70.0 to 90.3 Mg DW ha<sup>-1</sup> y<sup>-1</sup> (Azman et al., 2021; Hickey et al., 2018; Khan et al., 2009; Komiyama et al., 2008), but overall lower than reported AGB in tropical mangroves ranging from 116.0 to 246.9 Mg DW ha<sup>-1</sup> y<sup>-1</sup> (Fatoyinbo & Simard, 2013; Otero et al., 2018; Salum et al., 2020; Tang et al., 2016). Although the dissimilarity among these mangrove AGB is caused by a number of biotic and abiotic factors instead of any single factor, previous studies have highlighted the important role of several factors including latitude/temperature (Saenger & Snedaker, 1993), species types (Azman et al., 2021) and stand age (Lucas

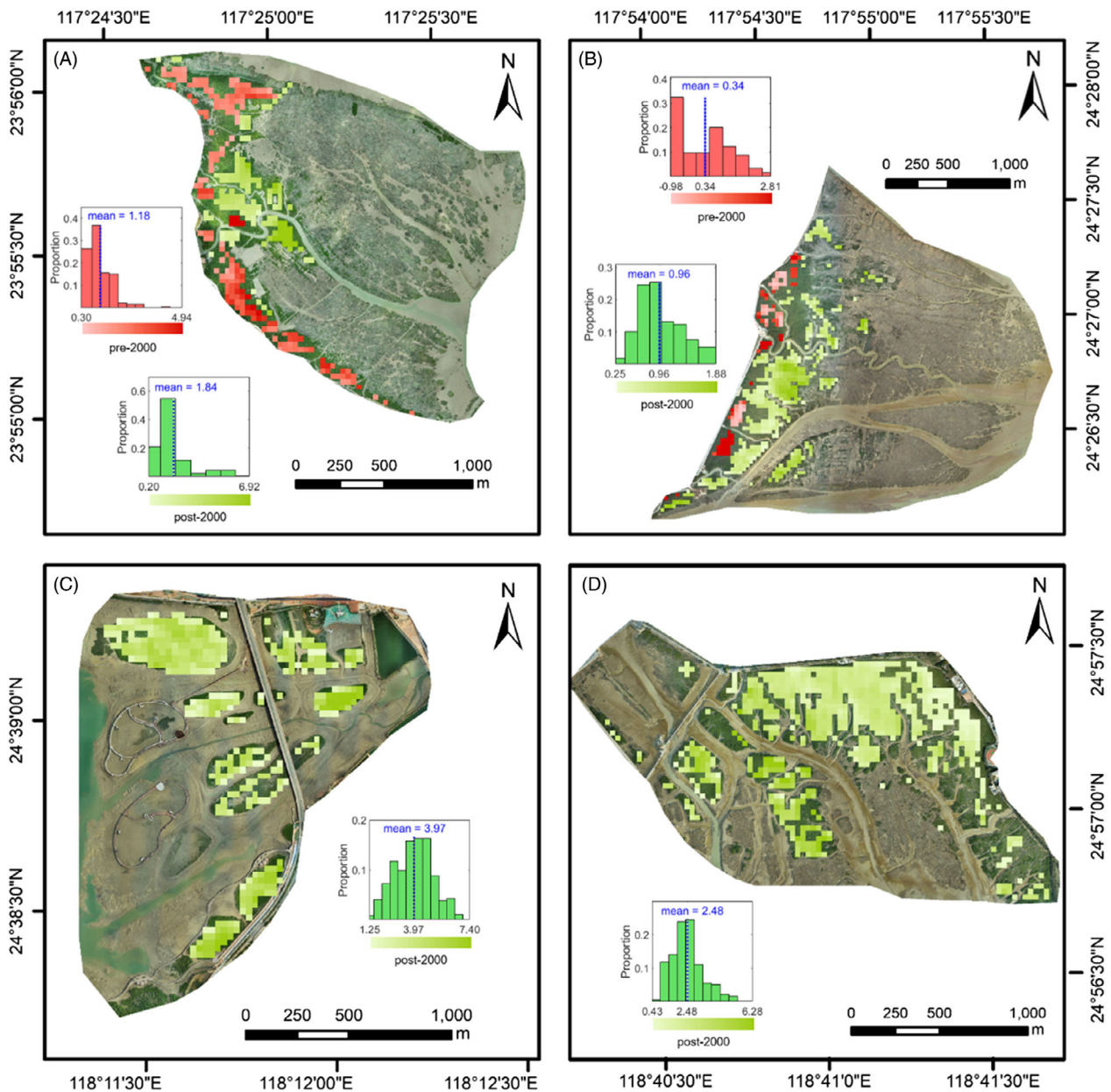


**Figure 7.** Spatial distributions of annual AGB accumulation rates ( $\text{Mg DW ha}^{-1} \text{y}^{-1}$ ) during the young growth stage of mangroves in four sites: (A) ZJE, (B) JRE, (C) XMB and (D) QZB. Annual accumulation rates were mapped for the pre-2000 (for ZJE and JRE only) and post-2000 conservation periods. The histograms of annual accumulation rates were also shown with horizontal color bars and corresponding variation ranges matching the maps. Mangrove pixels with stand age  $< 35$  years and annual accumulation rates statistically significant ( $P < 0.05$ ) were shown only.

et al., 2020) in determining the spatial and temporal variations in mangrove AGB.

The magnitudes of annual AGB accumulation rates during the young growth stage of mangroves over the pre-2000 and post-2000 conservation periods in these four sites are comparable with those in previous studies ranging from 2.48 to  $6.16 \text{ Mg DW ha}^{-1} \text{y}^{-1}$  (Thi Kim Cuc & Thi Hien, 2021); Castañeda-Moya et al. (2013)

The reasons why annual accumulation rates of mangrove AGB are higher over the post-2000 period than the pre-2000 period are multifaceted but at least related to the following aspects. First, the Chinese government has made great efforts to establish mangrove natural reserves and special laws to protect mangrove ecosystems (Chen et al., 2009; Jia et al., 2018). In fact, stronger mangrove conservation and restoration efforts have been put into

effect since 2000 along the coast of China, and thus the area of mangrove forests recovers rapidly in the past two decades (Hu et al., 2018; Jia et al., 2018; Wang et al., 2020b). Among the four mangrove sites in this study, in 2003, QZB was set as a provincial nature reserve and ZJE was promoted from a provincial to the national nature reserve. Second, mangrove restorations in China are often implemented by planting mangrove seedlings consisted of single or just a few species, which may relieve the early growth stage of young mangroves from species competition (Azman et al., 2021; Jia et al., 2018). Third, monoculture mangroves from restoration tend to have spatially even stand age and thus may have low self-thinning effect during the young growth stage (Azman et al., 2021).

The developed remote sensing approach for mapping annual mangrove AGB from Landsat EVI makes it possible to conduct spatially explicit analyses of AGB accumulation. The assessments of mangrove conservation effects from these analyses suffer from several uncertainties. First, although the uniform exponential equation is used to describe the relationship between Landsat EVI and canopy height, this remote sensing equation only partially explains the variability. Further improvement of this equation is needed in future studies possibly by incorporating other remote sensing-derived impact factors such as species composition (Zhu et al., 2019), forest gap (Liu et al., 2017) and tidal regime (Xia et al., 2020). Second, the linear height-AGB equation is used for formulating the remote sensing approach of AGB estimations in this study, but the uncertainty in applying this simple allometric equation should be further assessed with more available field data in the future (Fatoyinbo & Simard, 2013). Third, although these four mangrove sites have similar species compositions with relatively low spatial heterogeneity, the inconsistency in the spatial resolution of different data (Landsat and UAV) and the mixed pixel issue within the Landsat footprint also lead to uncertainty in the assessments. Lastly, the applicability of space-for-time method in these mangrove sites is an essential prerequisite for estimating mangrove AGB, but the space-for-time method may also lead to the misinterpretation of temporal dynamics (Walcker et al., 2018; Walker et al., 2010). Future studies with independent data on the long-term growth dynamics of mangrove forests are needed to further confirm the reliability of the empirical growth curves.

## Conclusions

A novel remote sensing approach using readily available UAV and Landsat data is proposed in this study to assess the spatial evolution of AGB accumulation of young

mangroves. The approach applies an empirical EVI-height-AGB equation to conduct spatially explicit assessments of mangrove conservation effects in terms of AGB accumulation for four subtropical estuarine mangroves in the southeastern coast of China. The main findings are summarized as follows. (1) The UAV-SfM technology serves as an effective and low-cost means for capturing the spatial heterogeneity of mangrove canopy heights. (2) The space-for-time analyses confirms that a maximum stand age of 15 years can be used to define the young growth stage of mangroves, for which the EVI-height relationships can be described by exponential equations without suffering significant spectral saturation effects. (3) Mangrove forests have overall faster annual AGB accumulation during the young growth stage over the post-2000 *versus* pre-2000 conservation period.

This is one of the first attempts to develop a remote sensing approach for analyzing decade-scale AGB accumulations of young mangroves in a spatially explicit manner. This study highlights the practicability and advantage of the UAV-SfM technology and confirms that stronger conservation efforts promote mangrove AGB accumulation in the past two decades. The EVI-height-AGB framework fueled with readily available UAV and Landsat data provides a unique tool for assessing mangrove conservation effects from landscape to regional scales.

## Acknowledgements

We are grateful to staff at Zhangjiang Estuary Mangrove National Nature Reserve for their help in the fieldwork. This research was funded by the Special Project on National Science and Technology Basic Resources Investigation of China (2021FY100704), the Natural Science Foundation of Fujian Province, China (2020 J01112079), the Youth Innovation Foundation of Xiamen, China (3502Z20206038), Fuzhou Science and Technology Bureau (2021-N-123) and the Fundamental Research Funds for the Central Universities of China (20720210075). The authors declare no conflict of interest. The funders had no role in the design of the study, in the collection, analyses, or interpretation of data, in the writing of the manuscript, or in the decision to publish the results.

## Authors' Contributions

X. Zhu was involved in conceptualization. Z. Zhu, M. Huang, Z. Zhou, G. Huang and X. Zhu carried out methodology, investigation, and formal analysis. Z. Zhu and X. Zhu contributed to the writing and reviewing of the manuscript. X. Zhu carried out project administration and funding acquisition.

## Data Availability Statement

The remote sensing data used in this study can be acquired from the corresponding author upon reasonable request.

## References

- Aksornkoae, S. (1982) In: Kostermans, A.Y. & Sastroutomo, S.S. (Eds.) *Productivity and energy relationships of mangrove plantations of *Rhizophora apiculata* in Thailand. Symposium on mangrove forest ecosystem productivity in Southeast Asia*. Bogor, Indonesia: Biotrop special publications, pp. 25–31.
- Alongi, D. (2009) *The energetics of mangrove forests*. Netherlands: Springer.
- Azman, M.S., Sharma, S., Shaharudin, M.A.M., Hamzah, M.L., Adibah, S.N., Zakaria, R.M. et al. (2021) Stand structure, biomass and dynamics of naturally regenerated and restored mangroves in Malaysia. *Forest Ecology and Management*, **482**, 118852.
- Barbier, E.B. (2016) The protective service of mangrove ecosystems: a review of valuation methods. *Marine Pollution Bulletin*, **109**(2), 676–681.
- Berveglieri, A., Imai, N.N., Christovam, L.E., Galo, M.L.B.T., Tommaselli, A.M.G. & Honkavaara, E. (2021) Analysis of trends and changes in the successional trajectories of tropical forest using the Landsat NDVI time series. *Remote Sensing Applications: Society and Environment*, **24**, 100622.
- Blois, J.L., Williams, J.W., Fitzpatrick, M.C., Jackson, S.T. & Ferrier, S. (2013) Space can substitute for time in predicting climate-change effects on biodiversity. *Proceedings of the National Academy of Sciences*, **110**(23), 9374.
- Castañeda-Moya, E., Twilley, R.R. & Rivera-Monroy, V.H. (2013) Allocation of biomass and net primary productivity of mangrove forests along environmental gradients in the Florida Coastal Everglades, USA. *Forest Ecology and Management*, **307**, 226–241.
- Castillo, J.A.A., Apan, A.A., Maraseni, T.N. & Salmo, S.G., III. (2017) Estimation and mapping of above-ground biomass of mangrove forests and their replacement land uses in The Philippines using sentinel imagery. *ISPRS Journal of Photogrammetry and Remote Sensing*, **134**, 70–85.
- Chen, B., Xiao, X., Li, X., Pan, L., Doughty, R., Ma, J. et al. (2017) A mangrove forest map of China in 2015: analysis of time series Landsat 7/8 and sentinel-1A imagery in Google earth engine cloud computing platform. *ISPRS Journal of Photogrammetry and Remote Sensing*, **131**, 104–120.
- Chen, L., Wang, W., Zhang, Y. & Lin, G. (2009) Recent progresses in mangrove conservation, restoration and research in China. *Journal of Plant Ecology*, **2**(2), 45–54.
- Dandois, J.P. & Ellis, E.C. (2010) Remote sensing of vegetation structure using computer vision. *Remote Sensing*, **2**(4), 1157–1176.
- Dandois, J.P. & Ellis, E.C. (2013) High spatial resolution three-dimensional mapping of vegetation spectral dynamics using computer vision. *Remote Sensing of Environment*, **136**, 259–276.
- Davis, J.H.J. 1940. The ecology and geological role of mangroves in Florida in Carnegie Inst. Wash. Publ. **32**, 306–412.
- Dittmar, T., Hertkorn, N., Kattner, G. & Lara, R.J. (2006) Mangroves, a major source of dissolved organic carbon to the oceans. *Global Biogeochemical Cycles*, **20**(1), GB1012.
- Donato, D.C., Kauffman, J.B., Murdiyarso, D., Kurnianto, S., Stidham, M. & Kanninen, M. (2011) Mangroves among the most carbon-rich forests in the tropics. *Nature Geoscience*, **4**(5), 293–297.
- Doughty, C.L., Ambrose, R.F., Okin, G.S., Cavanaugh, K.C., Disney, M. & De Angelo, C. (2021) Characterizing spatial variability in coastal wetland biomass across multiple scales using UAV and satellite imagery. *Remote Sensing in Ecology and Conservation*, **7**(3), 411–429.
- Farzanmanesh, R., Khoshelham, K. & Thomas, S. (2021) Technological opportunities for measuring and monitoring blue carbon initiatives in mangrove ecosystems. *Remote Sensing Applications: Society and Environment*, **24**, 100612.
- Fatoyinbo, T.E. & Simard, M. (2013) Height and biomass of mangroves in Africa from ICESat/GLAS and SRTM. *International Journal of Remote Sensing*, **34**(2), 668–681.
- Ferreira, A.C., Ganade, G. & Luiz de Atayde, J. (2015) Restoration versus natural regeneration in a neotropical mangrove: effects on plant biomass and crab communities. *Ocean and Coastal Management*, **110**, 38–45.
- Foga, S., Scaramuzza, P.L., Guo, S., Zhu, Z., Dilley, R.D., Beckmann, T. et al. (2017) Cloud detection algorithm comparison and validation for operational Landsat data products. *Remote Sensing of Environment*, **194**, 379–390.
- Giri, C., Ochieng, E., Tieszen, L.L., Zhu, Z., Singh, A., Loveland, T. et al. (2011) Status and distribution of mangrove forests of the world using earth observation satellite data. *Global Ecology and Biogeography*, **20**(1), 154–159.
- Gregorczyk, A. (1991) A logistic function—its application to the description and prognosis of plant growth. *Acta Societatis Botanicorum Poloniae*, **60**, 67–76.
- Hickey, S.M., Callow, N.J., Phinn, S., Lovelock, C.E. & Duarte, C.M. (2018) Spatial complexities in aboveground carbon stocks of a semi-arid mangrove community: a remote sensing height-biomass-carbon approach. *Estuarine, Coastal and Shelf Science*, **200**, 194–201.
- Hu, L., Li, W. & Xu, B. (2018) Monitoring mangrove forest change in China from 1990 to 2015 using Landsat-derived spectral-temporal variability metrics. *International Journal of Applied Earth Observation and Geoinformation*, **73**, 88–98.
- Hu, T., Zhang, Y., Su, Y., Zheng, Y., Lin, G. & Guo, Q. (2020) Mapping the global mangrove Forest aboveground biomass

- using multisource remote sensing data. *Remote Sensing*, **12** (10), 1690.
- Huete, A., Didan, K., Miura, T., Rodriguez, E.P., Gao, X. & Ferreira, L.G. (2002) Overview of the radiometric and biophysical performance of the MODIS vegetation indices. *Remote Sensing of Environment*, **83**(1), 195–213.
- James, G.K., Adegoke, J.O., Osagie, S., Ekechukwu, S., Nwilo, P. & Akinyede, J. (2013) Social valuation of mangroves in The Niger Delta region of Nigeria. *International Journal of Biodiversity Science, Ecosystem Services & Management*, **9**(4), 311–323.
- Jia, M., Wang, Z., Mao, D., Huang, C. & Lu, C. (2021) Spatial-temporal changes of China's mangrove forests over the past 50 years: an analysis towards the sustainable development goals (SDGs). *Chinese Science Bulletin*, **66**(30), 3886–3901.
- Jia, M., Wang, Z., Zhang, Y., Mao, D. & Wang, C. (2018) Monitoring loss and recovery of mangrove forests during 42 years: the achievements of mangrove conservation in China. *International Journal of Applied Earth Observation and Geoinformation*, **73**, 535–545.
- Jones, A.R., Segaran, R.R., Clarke, K.D., Waycott, M., Goh, W.S.H. & Gillanders, B.M. (2020) Estimating mangrove tree biomass and carbon content: A comparison of Forest inventory techniques and drone imagery. *Frontiers in Marine Science*, **6**, 784.
- Kauffman, J.B., Heider, C., Norfolk, J. & Payton, F. (2014) Carbon stocks of intact mangroves and carbon emissions arising from their conversion in The Dominican Republic. *Ecological Applications*, **24**(3), 518–527.
- Khan, M.N.I., Suwa, R. & Hagihara, A. (2009) Biomass and aboveground net primary production in a subtropical mangrove stand of *Kandelia obovata* (S., L.) Yong at Manko wetland, Okinawa, Japan. *Wetlands Ecology and Management*, **17**(6), 585–599.
- Kirwan, M.L. & Megonigal, J.P. (2013) Tidal wetland stability in the face of human impacts and sea-level rise. *Nature*, **504** (7478), 53–60.
- Klemas, V. (2013) Remote sensing of coastal wetland biomass: an overview. *Journal of Coastal Research*, **29**(5), 1016–1028.
- Komiyama, A., Ong, J.E. & Pongpan, S. (2008) Allometry, biomass, and productivity of mangrove forests: a review. *Aquatic Botany*, **89**(2), 128–137.
- Lechner, A.M., Foody, G.M. & Boyd, D.S. (2020) Applications in remote sensing to Forest ecology and management. *One Earth*, **2**(5), 405–412.
- Lee, H. (2008) Mapping deforestation and age of Evergreen trees by applying a binary coding method to time-series Landsat November images. *IEEE Transactions on Geoscience and Remote Sensing*, **46**(11), 3926–3936.
- Liu, M., Li, H., Li, L., Man, W., Jia, M., Wang, Z. et al. (2017) Monitoring the invasion of *Spartina alterniflora* using multi-source high-resolution imagery in the Zhangjiang estuary, China. *Remote Sensing*, **9**(6), 539.
- Lu, D. (2005) Aboveground biomass estimation using Landsat TM data in the Brazilian Amazon. *International Journal of Remote Sensing*, **26**(12), 2509–2525.
- Lu, D., Chen, Q., Wang, G., Moran, E., Batistella, M., Zhang, M. et al. (2012) Aboveground Forest biomass estimation with Landsat and LiDAR data and uncertainty analysis of the estimates. *International Journal of Forestry Research*, **2012**, 436537.
- Lucas, R., Van De Kerchove, R., Otero, V., Lagomasino, D., Fatoyinbo, L., Omar, H. et al. (2020) Structural characterisation of mangrove forests achieved through combining multiple sources of remote sensing data. *Remote Sensing of Environment*, **237**, 111543.
- Masek, J.G., Vermote, E.F., Saleous, N.E., Wolfe, R., Hall, F.G., Huemmrich, K.F. et al. (2006) A Landsat surface reflectance dataset for North America, 1990–2000. *IEEE Geoscience and Remote Sensing Letters*, **3**(1), 68–72.
- Messinger, M., Asner, G.P. & Silman, M. (2016) Rapid assessments of Amazon Forest structure and biomass using small unmanned aerial systems. *Remote Sensing*, **8** (8), 615.
- Navarro, A., Young, M., Allan, B., Carnell, P., Macreadie, P. & Ierodiaconou, D. (2020) The application of unmanned aerial vehicles (UAVs) to estimate above-ground biomass of mangrove ecosystems. *Remote Sensing of Environment*, **242**, 111747.
- Otero, V., Van De Kerchove, R., Satyanarayana, B., Martínez-Espinosa, C., Fisol, M.A.B., Ibrahim, M.R.B. et al. (2018) Managing mangrove forests from the sky: Forest inventory using field data and unmanned aerial vehicle (UAV) imagery in the Matang mangrove Forest reserve, peninsular Malaysia. *Forest Ecology and Management*, **411**, 35–45.
- Pflugmacher, D., Cohen, W.B., Kennedy, R.E. & Yang, Z. (2014) Using Landsat-derived disturbance and recovery history and lidar to map forest biomass dynamics. *Remote Sensing of Environment*, **151**, 124–137.
- Pham, T.D., Yokoya, N., Bui, D.T., Yoshino, K. & Friess, D.A. (2019) Remote sensing approaches for monitoring mangrove species, structure, and biomass: opportunities and challenges. *Remote Sensing*, **11**(3), 230.
- Potapov, P.V., Turubanova, S.A., Hansen, M.C., Adusei, B., Broich, M., Altstatt, A. et al. (2012) Quantifying forest cover loss in Democratic Republic of the Congo, 2000–2010, with Landsat ETM+ data. *Remote Sensing of Environment*, **122**, 106–116.
- Saenger, P. & Snedaker, S.C. (1993) Pantropical trends in mangrove above-ground biomass and annual litterfall. *Oecologia*, **96**(3), 293–299.
- Salum, R.B., Souza-Filho, P.W.M., Simard, M., Silva, C.A., Fernandes, M.E.B., Cougo, M.F. et al. (2020) Improving mangrove above-ground biomass estimates using LiDAR. *Estuarine, Coastal and Shelf Science*, **236**, 106585.
- Sankey, T., Donager, J., McVay, J. & Sankey, J.B. (2017) UAV lidar and hyperspectral fusion for forest monitoring in the

- southwestern USA. *Remote Sensing of Environment*, **195**, 30–43.
- Schonberger, J.L. & Frahm, J.M. (2016) Structure-from-motion revisited. In: *Proceedings of the IEEE conference on computer vision and pattern recognition, IEEE*, pp. 4104–4113.
- Shinozaki, K. (1961) Logistic theory of plant growth. Ph. D. Thesis. Kyoto Univ.
- Tang, W., Feng, W., Jia, M., Shi, J., Zuo, H. & Trettin, C.C. (2016) The assessment of mangrove biomass and carbon in West Africa: a spatially explicit analytical framework. *Wetlands Ecology and Management*, **24**(2), 153–171.
- Thi Kim Cuc, N. & Thi Hien, H. (2021) Stand structure and above ground biomass of *Kandelia obovata* Sheue, H.Y. Liu & J. Yong mangrove plantations in northern, Viet Nam. *Forest Ecology and Management*, **483**, 118720.
- Uddin, M., de Ruyter van Steveninck, E., Stuij, M. & Shah, M.A.R. (2015) Economic valuation of provisioning and cultural services of a protected mangrove ecosystem: A case study on Sundarbans reserve forest, Bangladesh. *Ecosystem Services*, **5**, 88–93.
- Vanderklift, M.A., Marcos-Martinez, R., Butler, J.R.A., Coleman, M., Lawrence, A., Prislán, H. et al. (2019) Constraints and opportunities for market-based finance for the restoration and protection of blue carbon ecosystems. *Marine Policy*, **107**, 103429.
- Vermote, E., Justice, C., Claverie, M. & Franch, B. (2016) Preliminary analysis of the performance of the Landsat 8/OLI land surface reflectance product. *Remote Sensing of Environment*, **185**, 46–56.
- Walcker, R., Gandois, L., Proisy, C., Corenblit, D., Mougin, E., Laplanche, C. et al. (2018) Control of “blue carbon” storage by mangrove ageing: evidence from a 66-year chronosequence in French Guiana. *Global Change Biology*, **24**(6), 2325–2338.
- Walker, L.R., Wardle, D.A., Bardgett, R.D. & Clarkson, B.D. (2010) The use of chronosequences in studies of ecological succession and soil development. *Journal of Ecology*, **98**(4), 725–736.
- Wang, D., Wan, B., Liu, J., Su, Y., Guo, Q., Qiu, P. et al. (2020a) Estimating aboveground biomass of the mangrove forests on Northeast Hainan Island in China using an upscaling method from field plots, UAV-LiDAR data and Sentinel-2 imagery. *International Journal of Applied Earth Observation and Geoinformation*, **85**, 101986.
- Wang, G., Yu, C., Singh, M., Guan, D., Xiong, Y., Zheng, R. et al. (2021) Community structure and ecosystem carbon stock dynamics along a chronosequence of mangrove plantations in China. *Plant and Soil*, **464**, 605–620.
- Wang, L., Jia, M., Yin, D. & Tian, J. (2019) A review of remote sensing for mangrove forests: 1956–2018. *Remote Sensing of Environment*, **231**, 111223.
- Wang, M., Cao, W., Guan, Q., Wu, G. & Wang, F. (2018) Assessing changes of mangrove forest in a coastal region of Southeast China using multi-temporal satellite images. *Estuarine, Coastal and Shelf Science*, **207**, 283–292.
- Wang, W., Fu, H., Lee, S.Y., Fan, H. & Wang, M. (2020b) Can strict protection stop the decline of mangrove ecosystems in China? From rapid destruction to rampant degradation. *Forests*, **11**(1), 55.
- Warfield, A.D. & Leon, J.X. (2019) Estimating mangrove forest volume using terrestrial laser scanning and UAV-derived structure-from-motion. *Drones*, **3**(2), 3020032.
- Waring, R.H., Milner, K.S., Jolly, W.M., Phillips, L. & McWethy, D. (2006) Assessment of site index and forest growth capacity across the Pacific and inland Northwest U.S.A. with a MODIS satellite-derived vegetation index. *Forest Ecology and Management*, **228**(1–3), 285–291.
- Xia, Q., Qin, C.-Z., Li, H., Huang, C., Su, F.-Z. & Jia, M.-M. (2020) Evaluation of submerged mangrove recognition index using multi-tidal remote sensing data. *Ecological Indicators*, **113**, 106196.
- Younes, N., Northfield, T.D., Joyce, K.E., Maier, S.W., Duke, N.C. & Lymburner, L. (2020) A novel approach to modelling mangrove phenology from satellite images: A case study from northern Australia. *Remote Sensing*, **12**(24), 4008.
- Zarco-Tejada, P.J., Diaz-Varela, R., Angileri, V. & Loudjani, P. (2014) Tree height quantification using very high resolution imagery acquired from an unmanned aerial vehicle (UAV) and automatic 3D photo-reconstruction methods. *European Journal of Agronomy*, **55**, 89–99.
- Zhao, C. & Qin, C.-Z. (2020) 10-m-resolution mangrove maps of China derived from multi-source and multi-temporal satellite observations. *ISPRS Journal of Photogrammetry and Remote Sensing*, **169**, 389–405.
- Zhu, X., Hou, Y., Weng, Q. & Chen, L. (2019) Integrating UAV optical imagery and LiDAR data for assessing the spatial relationship between mangrove and inundation across a subtropical estuarine wetland. *ISPRS Journal of Photogrammetry and Remote Sensing*, **149**, 146–156.

## Supporting Information

Additional supporting information may be found online in the Supporting Information section at the end of the article.

### Supplementary Materials.